
Asymmetric Contrastive Multimodal Learning for Advancing Chemical Understanding

Hao Xu^{1,†}, Yifei Wang^{1,†}, Yunrui Li^{1,†}, Pengyu Hong^{1,*}

¹Department of Computer Science, Brandeis University, Waltham, MA, USA

* Corresponding author † Equal contribution

{haox, yifeiwang, yunruili, hongpeng}@brandeis.edu

Abstract

The versatility of multimodal deep learning holds tremendous promise for advancing scientific research and practical applications. As this field continues to evolve, the collective power of cross-modal analysis promises to drive transformative innovations, leading us to new frontiers in chemical understanding and discovery. Hence, we introduce **Asymmetric Contrastive Multimodal Learning** (ACML) as a novel approach tailored for molecules, showcasing its potential to advance the field of chemistry. ACML harnesses the power of effective asymmetric contrastive learning to seamlessly transfer information from various chemical modalities to molecular graph representations. By combining pre-trained chemical unimodal encoders and a shallow designed graph encoder, ACML facilitates the assimilation of coordinated chemical semantics from different modalities, leading to comprehensive representation learning with efficient training. This innovative framework enhances the interpretability of learned representations and bolsters the expressive power of graph neural networks. Through practical tasks such as isomer discrimination and uncovering crucial chemical properties for drug discovery, ACML exhibits its capability to revolutionize chemical research and applications, providing a deeper understanding of chemical semantics of different modalities.

Keywords: Multimodal Learning, Graph Representation Learning, Molecules, Asymmetric Contrastive Learning, Interpretability.

1 Introduction

Multimodal deep learning (MMDL) is a thriving and interdisciplinary research field that is dedicated to enhancing artificial intelligence (AI) capabilities in comprehending, reasoning, and deducing valuable information across various communicative modalities [1]. It serves as an effective approach for the communication and integration of diverse data sources (text, images, audio, video, sensor data, etc), inspiring the innovative creation of more accurate and powerful AI models. For example, DALL-E2 [2] can showcase substantial progress in image generation and modification given a short text prompt. Witnessing the recent surge of research in image and video comprehension [3, 4], text-to-image generation [2, 5], and embodied autonomous agents [6, 7], multidisciplinary research, including biology, chemistry, and physics, also starts to embrace multimodal deep learning to unlock profound insights into complex systems, tackle challenging scientific problems, and push the boundaries of knowledge [8–10].

In the realm of chemistry, MMDL has been extensively adapted to facilitate the representation learning across several chemical modalities, including chemical language, chemical notations, and molecular graphs [12–18]. It is essential to note that the potential of MMDL extends far beyond the above modalities [19]. For instance, the molecular graphical depiction (referred to as image in the rest of the

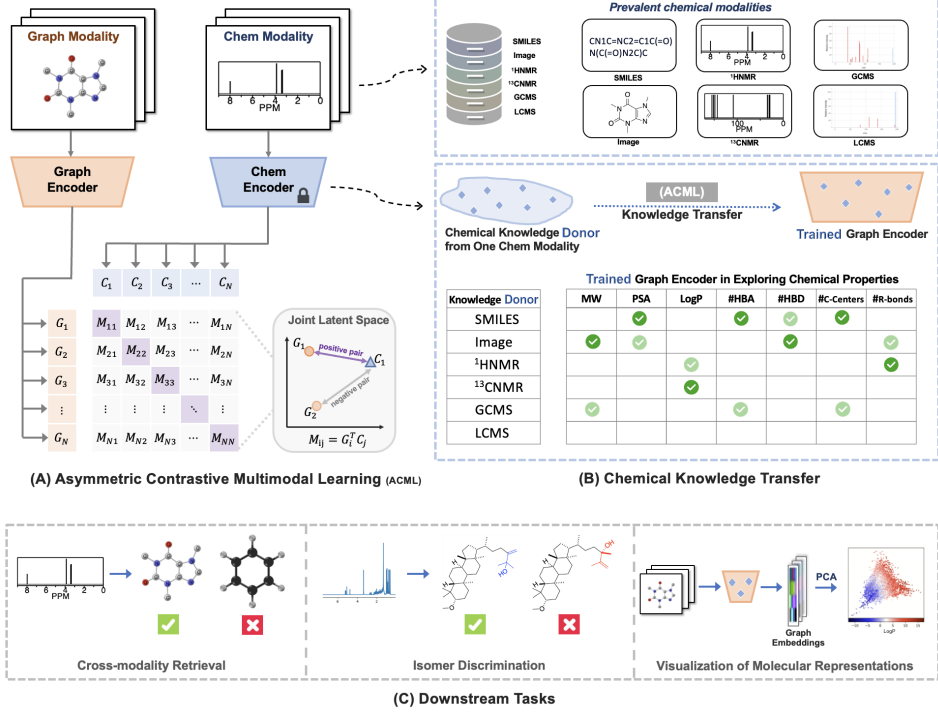


Figure 1: The framework of ACML (Asymmetric Contrastive Multimodal Learning). **a. The conceptual view of ACML.** Multimodal learning on multiple pairs of graph-chemical modality (Smiles, Images, NMR or Mass spectrometry) is established through asymmetric CLIP architecture [11]. The graph encoder is trained through ACML, while the encoder of chemical modality is pretrained and exempted from training. Embeddings from two modalities are projected into a joint latent space, aiming to align multiple views of the same molecule while distancing the embeddings from different molecules. **b. Chemical knowledge transfer in ACML.** For each chemical modality, an individual from-scratch graph encoder is paired and trained through the ACML framework, enabling it to express the learned chemical semantics from the corresponding chemical modality through latent embeddings. **c. Three downstream tasks** to demonstrate the effectiveness and interpretability of graph learning in ACML.

paper) [20] can offer powerful visual illustrations of molecules, providing unique insights into their spatial arrangements. Nuclear magnetic resonance (NMR) spectra, including ^1H NMR and ^{13}C NMR, offer a view of functional groups and characteristic features, enabling a deeper understanding of molecular behaviors and functionalities. Additionally, mass spectra from techniques such as gas chromatography–mass spectrometry (GCMS) and liquid chromatography–mass spectrometry (LCMS) provide a clue of molecular composition and fragmentation, aiding the identification and characterization of compounds. However, representing molecular information comprehensively using a single modality is a challenging task [21]. For example, string-based representations like SMILES [22] lack important topology information, whereas molecular depictions fail to include electronic information. MMDL could provide a solution by allowing the communication and integration of various heterogeneous modalities. However, there is limited work exploring such advantages in the chemical systems, transcending the limitations associated with each individual modality.

Among the implementations of MMDL, contrastive learning has emerged as one of the most prevalent self-supervised approaches for information communication across multiple modalities [23]. Its objective is to align multiple views of the same instance across modalities while distancing the representations from different instances. One typical approach is to adopt a coordinated mechanism, like CLIP (Contrastive Language-Image Pretraining) framework [11], to enhance multimodal communication. The coordinated model establishes correspondences between the learned representations by first projecting these representations onto a joint hidden space and then contrasting positive pairs (similar instances) against negative pairs (dissimilar instances). In the domain of chemistry, great

efforts have been directed towards using contrastive learning for tasks such as property predictions [14], unimodal pattern mining [24], and zero-shot classifications [19]. However, there remains a notable gap in research investigating the potential for integrating information across different modalities and elucidating the interpretability of learned representations within the context of multimodal coordination.

Many recent works have demonstrated strong advantages of molecular images [25], SMILES [26], and molecular graphs [27] to produce molecular representations for drug discovery. But what contributes to such superiority? It's important to recognize that the drug discovery process operates on multiple layers of informational hierarchy. These layers range from atomic-level properties such as hydrogen-bonding acceptors (HBA), to motif-level characteristics like hydrogen-bonding donors (HBD) and the number of stereogenic (chiral) centers, and finally to molecular-level attributes such as molecular weight, topological polar surface area (TPSA), and the logarithmic partition coefficient (logP). To answer the question, we may need to investigate how diverse modalities impact on these hierarchical properties.

In light of these opportunities, we propose a novel approach called Asymmetric Contrastive Multimodal Learning (ACML) specifically designed for molecules. It leverages contrastive learning between the molecular graph and other prevalent chemical modalities, including G-SMILES, G-image, G-¹HNMR, G-¹³CNMR, G-GCMS, and G-LCMS pairs (G for the abbreviation of Graph), to transfer the information from other chemical modalities into the graph representations in an asymmetric way. As graph representation can express hierarchical molecular information via carefully crafted graph neural networks (GNNs) [28–31], we regard it as a valuable receptor containing basic topology information of a given molecule to assimilate information from other modalities. ACML enables graph representation learning to capture knowledge across various chemical modalities, promoting a more holistic understanding of the hierarchical molecular information within diverse input chemical modalities. This multimodal learning framework not only enhances the interpretability of learned representations but also holds the potential to significantly improve the expressive power of graph neural networks within the field of chemistry. Figure 1 illustrates the conceptual view of the ACML framework.

In our proposed framework, each ACML model involves the graph encoder and one chemical unimodal encoder, for example, G-SMILES represents the multimodal learning between graph and SMILES modalities. We have a dedicated unimodal encoder for each modality. We maintain the graph encoder design simple and shallow to ensure efficient training. For the chemical modalities (SMILES, Image, ¹HNMR, ¹³CNMR, GCMS, and LCMS), we utilize pre-trained encoders and exempted them from training. Training of ACML allows the fixed chemical encoder to effectively transfer knowledge to graph encoders during asymmetric contrastive learning. Finally, we analyze and compare the embeddings generated by the trained graph encoders to discover their explanatory power. In summary, the advantages of our ACML can be viewed as follows:

1. Leverage effective asymmetric contrastive learning between graph and chemical modalities.
2. Achieve an efficient training scheme using the shallow graph encoder and pre-trained chemical encoders.
3. Empower knowledge transfer from chemical modalities into graph encoder during cross-modal chemical semantics learning.
4. Demonstrate the effectiveness and interpretability of graph learning in ACML, including three key tasks: (1) cross-modality retrieval (2) isomer discrimination, and (3) revealing important chemical properties relevant to drug discovery.

2 Results

2.1 ACML framework

The proposed ACML framework is built upon the contrastive learning framework inspired by [11]. It effectively promotes correspondences between modalities of the same molecule (positive pairs) while contrasting them of different molecules (negative pairs). The whole pipeline, elaborated in Section 4.1, is composed of four components: unimodal encoders for molecular modalities, graph encoder formalized by graph neural networks, non-linear projection head, and temperature-scaled cross-entropy contrastive loss.

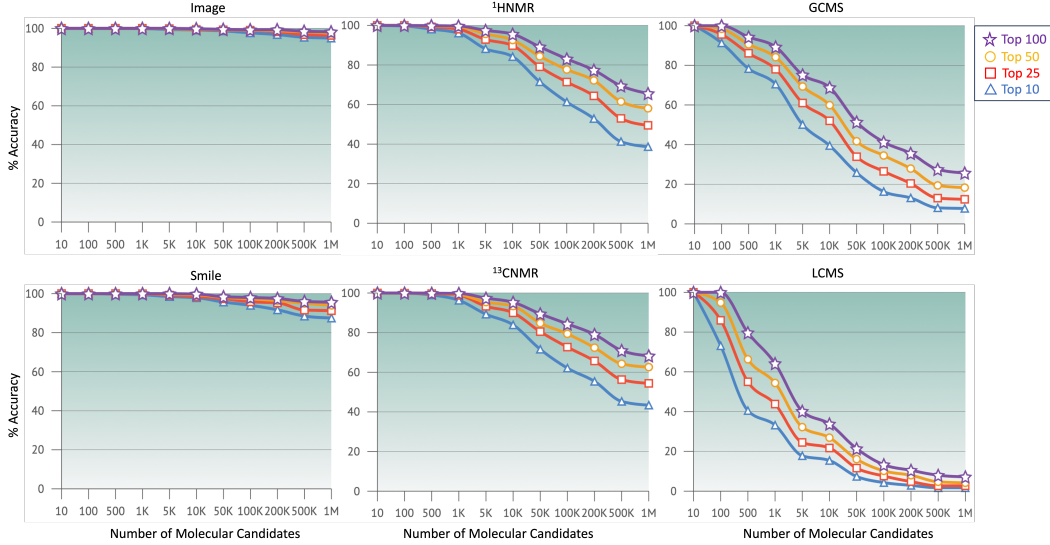


Figure 2: Cross-modality retrieval accuracy for all ACML models, including G-SMILES, G-image, G- 1 H NMR, G- 13 C NMR, G-GCMS, and G-LCMS. In each ACML model, the top k accuracy is calculated by matching one molecule’s chemical modality to its corresponding graph within a graph database of varying scales, from 1K to 1M.

Our ACML framework exhibits adaptability to diverse encoder designs, facilitating information extraction and compression. In our study, the encoders for each modality encompass Convolutional Neural Networks, trained to capture features for subsequent reconstruction tasks. Due to the inherent characteristics of each modality, the particulars of the encoder designs exhibit subtle variations. For instance, while 13 C NMR and 1 H NMR spectra both pertain to nuclear magnetic resonance, HNMR presents a higher degree of noise in comparison to 13 C NMR, along with a greater prevalence of peak overlap. In contrast, 13 C NMR peaks demonstrate enhanced distinctiveness. To address these disparities, 1 H NMR data may require some preprocessing to extract peak-related, condensed information which leads to a light-weight encoder that strategically aims at extracting pivotal features from the peaks. For 13 C NMR, the unaltered experimental data can be employed directly. The encoder architecture for 13 C NMR has more convolutional layers, tailored to capture intricate details.

2.2 Cross-modality retrieval

Molecules can be represented by a variety of modalities, such as depiction images, SMILES notations, and traditional chemical characterization techniques. However, each modality possesses distinct capabilities and constraints when it comes to deciphering molecular structures. In the context of structural attributes, molecular depiction image and isomeric SMILES notation offer a detailed overview of the whole molecule from atom level to molecule level, facilitating the elucidation of their three-dimensional atomic configurations. NMR spectra provide distinct windows into the carbon and hydrogen atomic landscapes of the molecule, offering partial structural information about the molecule. Mass spectra provide crucial information about molecular mass and patterns of fragmentation, encompassing both molecular-level and motif-level information. To evaluate each ACML model, we conduct a cross-modality retrieval task: determine whether the model can accurately match a chemical modality to its corresponding graph modality from a large database of molecular graphs. Higher retrieval accuracy indicates better multi-modal coordination between graph and chemical representations. Note that the sample in the graph database never appears in the training phase.

Figure 2 presents the retrieval accuracy results for all ACML models, including G-SMILES, G-image, G- 1 H NMR, G- 13 C NMR, G-GCMS, and G-LCMS. These results are obtained by calculating the top k accuracy when matching one molecule’s chemical modality to its corresponding graph within a graph database of varying scales. The task becomes more challenging as the scale increases. When the

scale transitions from 1 thousand (K) to 1 million (M), the G-Image gives the best results: the top 10 accuracy drops from 100% to 95.0%, which only experiences a reduction of 5.0%. G-SMILES gives the second best results, as top 10 accuracy drops from 100% to 87.5%. When it comes to G-¹HNMR, the results are not as good as G-Image and G-SMILES, as expected. Specifically, when the scale transitions from 1K to 10K, the top 10 accuracy drops from 96.1% to 84.2%. And with 1M unseen molecules, the top 10 accuracy is 38.7%. G-¹³CNMR spectrum exhibits similar performance, as the top 10 accuracy from 96.3% to 83.9% until 43.4% when the scale transitions from 1K to 10K and up to 1M. Notably, G-¹³CNMR performs better than G-¹HNMR when the search space expands. Intuitively, this aligns with the expectation, since the ¹³CNMR peaks are typically sharp and barely overlap in small molecules. On the contrary, the ¹HNMR spectrums are more prone to signal overlap, especially in complex molecular structures. Although the encoders of ¹³CNMR and ¹HNMR have been designed to cope with such differences, the training dataset inevitably falls short of encompassing the entirety of structural variations within the zero-shot validation set. Additionally, ¹HNMR might encounter sensitivity issues, especially for compounds with low hydrogen content. Nonetheless, both the G-¹HNMR and G-¹³CNMR exhibit satisfactory discrimination power in identifying the most probable graphs given the NMR sequences. This demonstrates the flexibility of our ACML framework with features from different spaces and dimensions generated from different designs of encoders.

When it comes to mass spectra modality, the results do not align as favorably as with images, smiles and NMR spectra, as initially anticipated. For G-GCMS, when the scale transitions from 1K to 10k, the top 10 accuracy experiences a certain degree of reduction from 70.5% to 39.5%. When the validation database extends to 1M, the top 10 accuracy dropped to 7.8%. For G-LCMS, when the scale transitions from 1K to 10K, the top 10 accuracy experiences a certain degree of reduction from 32.4% to 14.9%. When the validation database extends to 1M, the top 10 accuracy dropped to 1.7%. One may observe that G-GCMS has better performance on molecular recognition than G-LCMS. The reason for that is GCMS is typically carried out under harsh conditions, resulting in a wide array of fragmentation that unveils the molecular composition. In contrast, LCMS is generally performed under milder conditions, resulting in reduced fragmentation. Particularly, LC-MS/MS primarily concentrates on localized information near the precise molecular weight. However, in terms of cross-modality retrieval, LCMS offers less comprehensive information.

2.3 Isomer discrimination

Besides calculating accuracy among a large group of molecules, in which many molecules could be intrinsically different, isomer recognition stands as one of the most challenging tasks in molecular identification due to the intricacy of isomeric structures. Distinguishing between stereoisomers, which share the same connectivity but differ in spatial arrangement, poses a particular challenge and demands advanced analytical methods and meticulous data interpretation. Case studies have been conducted to demonstrate the capabilities of NMR modalities in terms of isomer recognition. From the validation set, several pairs of complex isomers has been picked up randomly. These isomers not only have identical formulas but also feature highly similar functional groups. In this investigation, both ¹³CNMR and ¹HNMR yield comparable results and effectively distinguish among the majority of instances. For each scenario, the ACML model is supplied with sets of NMRs, alongside confidence scores indicating the likelihood of these NMRs aligning with the corresponding pair of graphs. A greater confidence score signifies a stronger alignment according to our proposed framework. Four cases of ¹³CNMR are shown in Figure 3, where for each case, interested pairs of ¹³CNMR spectrum and possible molecular graphs are presented to the model. The model selects the molecule of the highest possibility to be the corresponding decipher of the ¹³CNMR spectrum. The proposed model correctly identifies 3 isomers out of 4. Similarly, four cases of ¹HNMR are shown in Figure 4, where for each case, interested pairs of ¹HNMR spectrum and possible molecular graphs are presented to the model. The proposed model correctly identifies 3 isomers out of 4.

2.4 Visualization of molecular representations

In the ACML framework, the graph modality serves as an information receptor capable of bringing forth the information or chemical rules from another modality via coordination. Thus, it may reveal distinct dimensions of chemical significance among diverse chemical modalities. To illuminate variations of chemical semantics embedded in hidden graph representations acquired from various ACML frameworks, we computed graph embeddings of previously unseen 30,000 molecules using

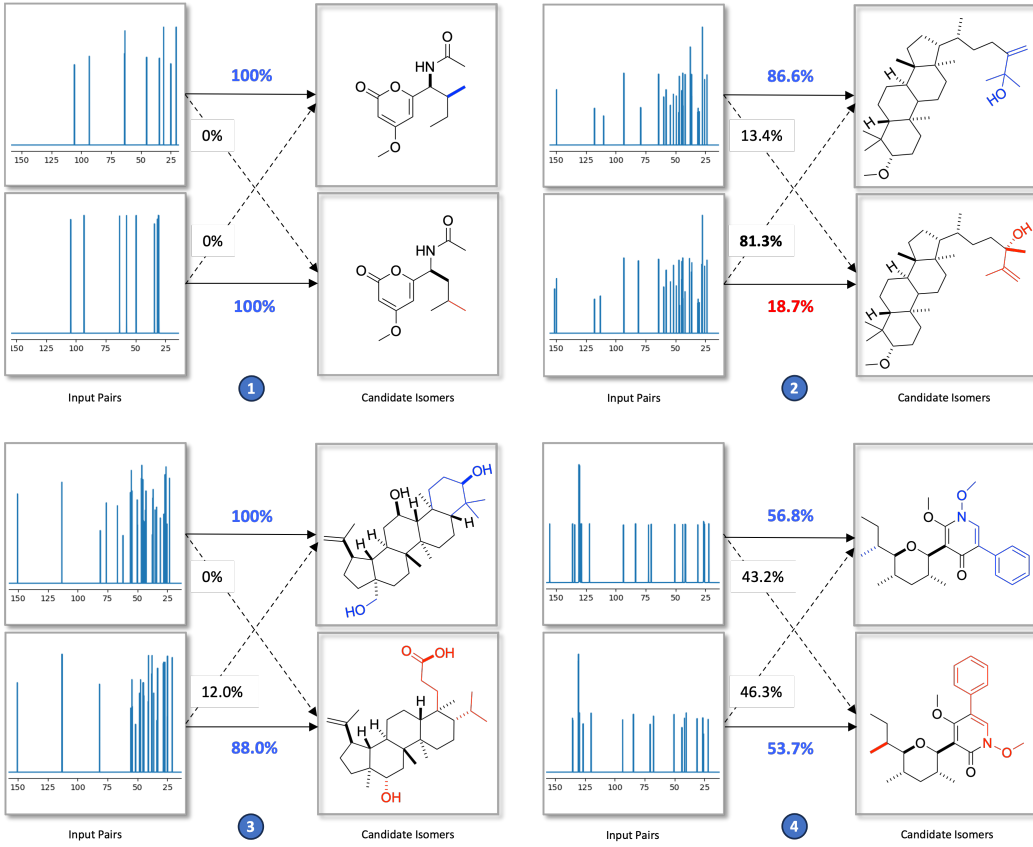


Figure 3: $^{13}\text{CNMR}$ Isomer discrimination task demonstrations. The correct pairs of $^{13}\text{CNMR}$ and molecule are presented horizontally, linked by solid arrows. Out of the 4 challenging isomer pairs, our proposed model correctly identifies 3 isomers.

pretrained graph encoders for analysis. In view of 8 important chemical characteristics in drug discovery: molecular weight (MW), LogP, HBA, HBD, the number of rotatable bonds, the number of stereogenic (chiral) centers, we decided to examine how these characteristics correlate with the graph embeddings. The scope of this inquiry extends to understanding the impact of these modalities on crucial parameters within the domain of drug discovery, highlighting the strengths of each molecular modality.

We decomposed the feature dimensions via PCA [32] and mapped these embeddings onto a two-dimensional plane. The outcomes were visualized as 2D points with coloring based on their corresponding chemical property values. Figure 5 presents the visualization results. Notably, a remarkable consistency in the distribution of points concerning the chemical property values was observed. This observation underscores the proficiency of the pre-trained graph encoder in capturing the inherent chemical semantics. We then conducted a quantitative evaluation of the relationship between graph embedding and the chemical properties using Pearson correlation coefficients (PCC) [33]. In our approach, we first established a linear regression model to determine the optimal linear combination of two PCA components that maximizes the Pearson correlation score between the linear combination of PCA components and chemical properties of interest. Table 2.4 presents the PCC scores of all ACML frameworks.

The advantages or capacities of the chemical modalities were captured and highlighted by the degree of correlation. Regarding **MW** (molecular weights), Image achieved the highest score, followed closely by GCMS. Molecular weights can effectively be expressed by the pixels of molecular depiction image, and extracted from mass spectrometry data provided by GCMS. This accounts for the superior performance of these two models in this context. For **HBA** (typically electronegative atoms with lone

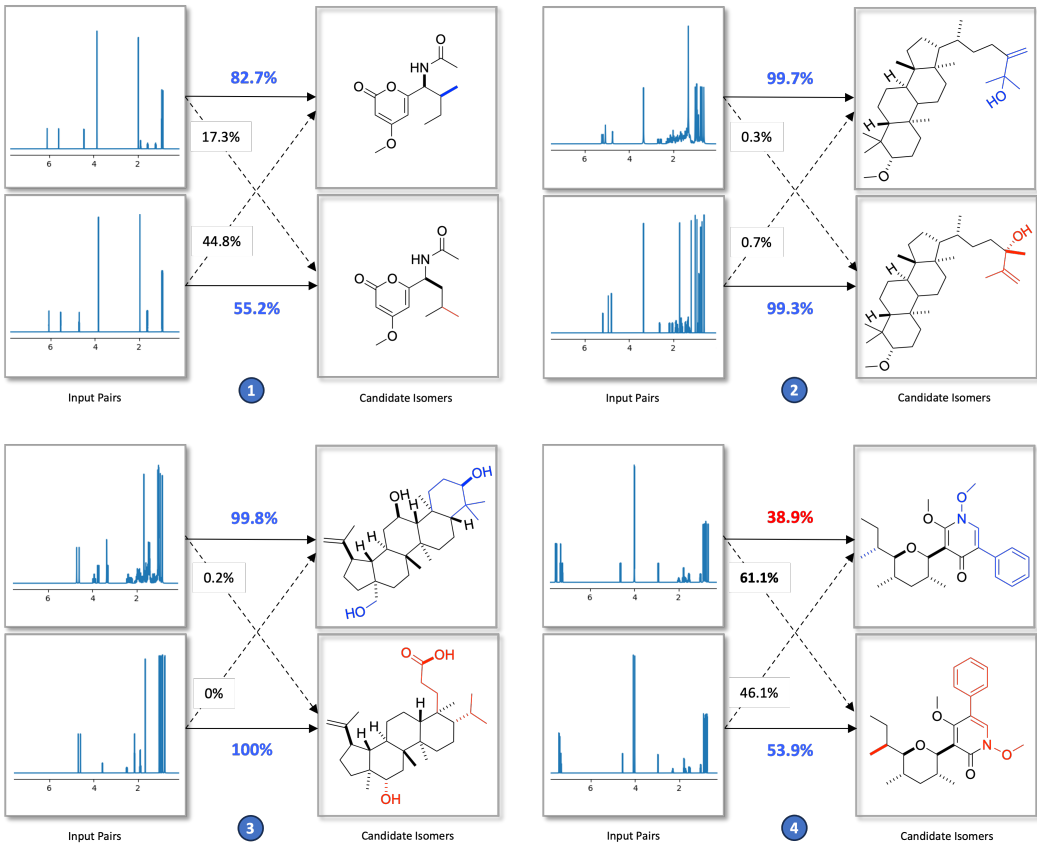


Figure 4: ^1H NMR Isomer discrimination demonstrations. The correct pairs of ^1H NMR and molecule are presented horizontally, linked by solid arrows. Out of the 4 challenging isomer pairs, our proposed model correctly identifies 3 isomers.

pairs), Smiles emerged as the top performer. It is expected because HBA atoms can be annotated by Smiles. For **HBD** (Hydrogen Bond Donor), Image demonstrates the best performances. In a hydrogen bond, the hydrogen bond donor donates its hydrogen atom to form a bond with a hydrogen bond acceptor. The hydrogen atom in the hydrogen bond donor is typically covalently bonded to a highly electronegative atom, such as oxygen (O), nitrogen (N), or fluorine (F). In the image, HBD is directly and explicitly presented in the image. On the contrary, hydrogens are not always contained in Smiles notation. Thus, Smiles has a slightly lower performance. In the case of **LogP**, ^{13}C NMR and ^1H NMR are the game winners. This outcome is attributable to the fact that LogP measures the solubility of a solute in both water and organic solvents, making it highly reliant on electronic information within the molecule. This electronic information is well captured by the two NMR techniques, and it remains concealed in other modalities such as Image, Smiles, or mass spectrometry. For **#R-Bonds** (the number of rotatable bonds), ^1H NMR exhibited the strongest performance, because the rotation of chemical bonds can be derived from the magnetic equivalence of vicinal and geminal protons. When considering **#C-Centers** (the number of Chiral centers), Smiles achieves the highest correlation coefficient of 0.8297. This strong correlation can be elucidated by the inherent advantage of Smiles: atoms with chiral centers are directly annotated in Smiles representations, that is, "@" represents chirality with inward direction and "@@" represents chirality with outward direction.

Remark 1. Note that PCC only measures the linear correlation while doesn't account for any nonlinear associations, a low PCC score doesn't necessarily imply a lack of correlation. For example, when we examined the embedding visualization of G- ^1H NMR for the "# Rotatable bond" task shown in Figure 5, we observed clear continuous color distributions, despite the PCC value being relatively low at 0.587.

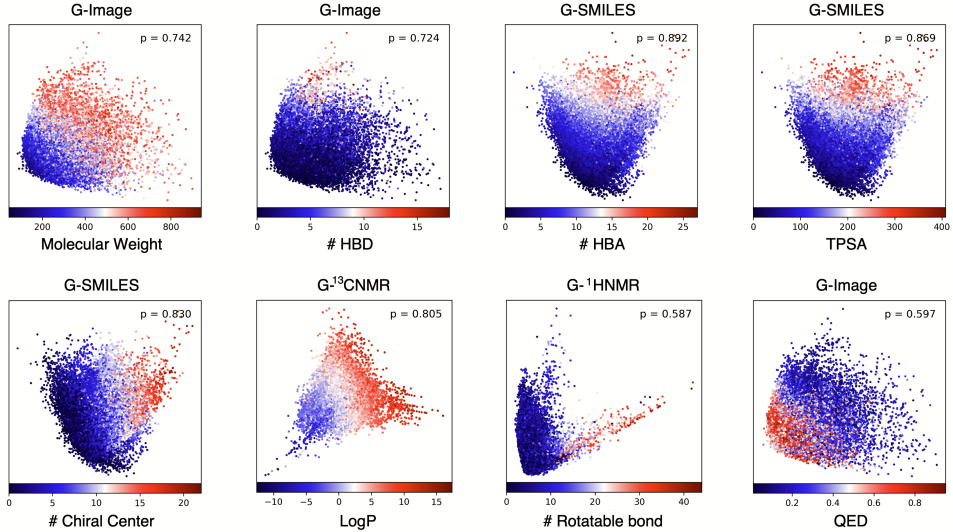


Figure 5: Graph embedding visualization via PCA.

Remark 2. These 8 chemical properties are very important in drug discovery. If the graph neural network is able to reveal this information, it offers the potential for deep models to understand the basic philosophy of molecular design and would even make breakthroughs in drug discovery. Note that these properties are never seen in ACML learning and the molecules we selected are also never seen in training, the surprising findings demonstrate our ACML framework is able to make a transition of chemical meaning to graph encoder, enhancing its interpretability.

	MW	#HBA	#HBD	LogP	PSA	#R-Bonds	#C-Centers	QED
G-Image	0.742	0.672	0.724	0.355	<u>0.736</u>	<u>0.325</u>	0.630	0.597
G-SMILES	0.623	0.892	<u>0.716</u>	0.564	0.869	0.244	0.830	<u>0.492</u>
G- ¹ HNMR	0.202	0.361	0.227	<u>0.588</u>	0.303	0.587	0.388	0.235
G- ¹³ CNMR	0.195	0.673	0.569	0.805	0.659	0.277	0.641	0.188
G-GCMS	<u>0.669</u>	<u>0.707</u>	0.499	0.312	0.659	0.055	<u>0.804</u>	0.409
G-LCMS	0.615	<u>0.254</u>	0.120	0.338	0.229	0.087	0.769	0.292

Table 1: Pearson correlation test results between graph representations and the chemical property of interest. Highest scores are marked as bold while the second highest are underlined. A higher score indicates that the low-dimensional graph representations have a higher linear correlation with the chemical property of interest.

3 Discussion and Conclusion

In this work, we introduce ACML framework, a novel approach tailored for molecular representational learning based on multi-modality contrastive learning. We demonstrate the inheritance of molecular graph-like structure allows graph representation to convey extensive information about molecules and treat the graph neural networks, i.e., the graph encoder, as a receptor to assimilate chemical semantics through multi-modal coordination, leading to effective and explainable molecular representational learning. Extensive experimental results on important chemical tasks such as isomer discrimination and uncovering crucial chemical properties for drug discovery demonstrate the cross-modality transfer ability and the power of graph neural networks.

Our findings reveal a series of interesting questions to consider: of particular interest is how to effectively train a graph encoder to make it tailored to molecular representational learning. Instead of designing a deep and complex GNN framework and proposing various levels of self-supervised tasks or effective pretraining, we demonstrate that through the use of multi-modality contrastive learning, a

shallow design of GNN with light training resources is able to produce an expressive graph encoder with good interpretability of 2D molecules.

The current framework exhibits certain room for further improvement. Firstly, this work is specifically tailored for 2D molecules. While we incorporate stereo information like chirality tags and stereo bond directions in the graph representations, complete geometric information from 3D molecular graphs is under-explored. We will leave the study of multi-modality learning on 3D molecules for future work. Secondly, we demonstrate the interpretability of learned graph representations by emphasizing their linear relation with several chemical properties, but the nonlinear relations is omitted. Additionally, we will continue to investigate how much the learned graph neural network could benefit downstream tasks for drug discovery.

4 Methods

4.1 The ACML framework

We propose a Contrastive Multimodal Representation Learning (ACML) framework for molecules, which mainly contains three parts: (1) unimodal encoder of chemical modality; (2) graph encoder; (3) projection modules. The goal is to map the hidden representations of the molecular graph and the chemical modality into the joint latent space.

First, the inputs of each ACML framework consist of a molecular graph modality and one chemical modality. For each chemical modality, we make use of effective pre-trained encoders from publicly available sources, which have been demonstrated to be effective in the corresponding downstream tasks (See Table 2). As for molecular graph representation, we employ the graph neural network (GNN) as the graph encoder, where we elaborated several GNN variants in Section 4.2. These inputs are then fed into their respective encoders to produce embeddings. Mathematically, let g and c denote a molecule’s graph representation and its chemical modality representation, their embeddings after passing to their corresponding encoders are:

$$\mathbf{h}_g = \text{ENCODER}_{\text{graph}}(g), \quad \mathbf{h}_c = \text{ENCODER}_{\text{chem}}(c) \quad (1)$$

It’s worth noting that $\mathbf{h}_g \in \mathbb{R}^{d_1}$ and $\mathbf{h}_c \in \mathbb{R}^{d_2}$ may have different dimensions, i.e., $d_1 \neq d_2$. To ensure that the information from two modalities could be coordinated in the same dimensional latent space, we apply two projection modules after both encoders. These modules assist in facilitating and coordinating between two modalities, resulting in the same dimensional hidden representations as projection outputs. In this study, the projection modules are designed as multiple-layer perceptrons (MLPs), which could be formulated as:

$$\mathbf{h}_g^{\text{proj}} = \text{MLP}_{\text{graph}}(\mathbf{h}_g), \quad \mathbf{h}_c^{\text{proj}} = \text{MLP}_{\text{chem}}(\mathbf{h}_c) \quad (2)$$

where $\mathbf{h}_g^{\text{proj}} \in \mathbb{R}^d$ and $\mathbf{h}_c^{\text{proj}} \in \mathbb{R}^d$ have the same dimension.

Unimodal	Representation	Encoder	Pre-trained Source
Image	2D image	CNN	Img2mol [20]
SMILES	Sequence	Transformer	CReSS [34]
^1H NMR	Sequence	1D CNN	N/A ^a
^{13}C NMR	Sequence	1D CNN	AutoEncoder [35]
GCMS & LCMS	Sequence	1D CNN	AutoEncoder [35]

^aThe ^1H NMR encoder undergoes pre-training using a CNN-based network similar to what’s described in [35]. Unlike the ^{13}C NMR and GCMS/LCMS encoders, the ^1H NMR encoder focuses on reducing the embedding dimensions to compress information while preserving satisfactory reconstruction ability. The diversity in encoder choices highlights the versatility of our suggested framework. This means encoders with varying degrees of modality information can be effectively integrated into the GNN network.

Table 2: Unimodal encoders of pervasive chemical modalities.

4.2 Graph encoder

Chemical molecules can be naturally represented as attributed relational graphs $G = (\mathcal{V}, \mathcal{E})$, where \mathcal{V} and \mathcal{E} are the node set and the edge set. Here a node $v \in \mathcal{V}$ and an edge $(v, u) \in \mathcal{E}$ represent the atom

v and the chemical bond connecting u and v , respectively. The corresponding atom features (atomic number, chirality tag, hybridization, etc.,) and bond features (bond types, stereotypes, etc.,) are treated as node attributes and edge attributes in the graph. Graph neural networks (GNNs) [36, 37] which operate on graphs, have been combined with deep learning [38] to learn representations on graph data [39–41]. GNNs are also demonstrated as effective frameworks for molecular representational learning [42, 29].

Graph convolution. Many popular graph convolutional frameworks follow the message-passing scheme, including an iterative way of updating node representations based on the aggregations from neighboring nodes. Widely used approaches, such as GCN [43], GIN [44], GAT [45] and GraphSage [46], all follow message passing schemes. For the rest of the paper, we refer “message passing based GNNs” as “GNN”. For simplicity, we denote $\mathbf{x}_u^{(k)}$ as node feature vector of node u in k -th layer, $\mathbf{e}_{v,u}$ as (optional) edge feature vector from node v to node u , and let \mathcal{N}_u represent the neighboring node set of the central node u . One message passing based convolution layer includes two steps: (1) create the message between the central node u and its neighbor v , formalized by the function $\phi^{(k)}(\mathbf{x}_u^{(k)}, \mathbf{x}_v^{(k)}, \mathbf{e}_{v,u})$; (2) aggregate the messages of all neighbors of the central node u using the operator \bigoplus , which denotes a differentiable and permutation invariant function, e.g., sum, mean or max operator. Mathematically, the latent node presentation is updated according to Equation 3 and will be fed into the next convolutional layer.

$$\mathbf{x}_u^{(k+1)} = f^{(k)}(\mathbf{x}_u^{(k)}, \bigoplus_{v \in \mathcal{N}(u)} \phi^{(k)}(\mathbf{x}_u^{(k)}, \mathbf{x}_v^{(k)}, \mathbf{e}_{v,u})) \quad (3)$$

where $f^{(k)}$ and $\phi^{(k)}$ denote differentiable functions like MLPs (Multi Layer Perceptrons). $\mathbf{x}_u^{(k+1)}$ is able to captures the structural information within its k -hop network neighborhood after k convolutional layers.

Graph pooling and readout. The node representations at the final iteration will be processed to generate the fixed-length graph-level representation \mathbf{h}_g , which involves graph pooling and readout operations. The pooling layer is usually applied to get a coarser graph which can be further reduced within a readout function, which is similar to conventional CNNs [47]. Actually, there is no strict distinction between pooling and readout operations in GNNs. Despite some studies [48, 49] that leveraged stacks of pooling layers for coarse graphs, most widely used works handling pooling and readout simultaneously by applying a permutation invariant function directly on all nodes in the graph to generate a fixed length graph representation [50–53], which is generally formalized as

$$\mathbf{h}_g = \text{READOUT}(\mathbf{x}_u^{(K)} \mid u \in \mathcal{V}) \quad (4)$$

The choice of aggregation operator. Many previous works [46, 44, 52, 54] demonstrate that the choice of aggregation function contributes significantly to the expressive power and performance of the model. In this work, we used sum operator in both message aggregation and graph readout function, which enables simple and effective learning of structural graph properties implied in [44, 30].

4.3 Multimodal contrastive learning

Instance discrimination is a versatile technique that can be harnessed to contrast representations in various ways: within the same modality, across different modalities, or even through a combination of both modalities, referring to “joint” instance discrimination [55, 56]. The target of ACML is to learn a joint embedding between two different modalities while at the same time ensuring that similar features from the same modality stay close-by in the joint embedding. Therefore, in the implementation of the contrastive loss mechanism we adopt across-modality instance discrimination [57]. This intermodal contrastive strategy proves to be particularly beneficial in scenarios where understanding relationships and translating knowledge across modalities is a primary objective.

Mathematically, given a mini-batch of N samples, $\{(g_1, c_1), (g_2, c_2), \dots, (g_N, c_N)\}$, where g_i represents the graph modality and c_i represents the chemical modality of the i -th molecule. According to Equ. 2, we denote $\{(\mathbf{h}_{g_1}^{\text{proj}}, \mathbf{h}_{c_1}^{\text{proj}}), (\mathbf{h}_{g_2}^{\text{proj}}, \mathbf{h}_{c_2}^{\text{proj}}), \dots, (\mathbf{h}_{g_N}^{\text{proj}}, \mathbf{h}_{c_N}^{\text{proj}})\}$ as the hidden representation vectors

after the projections. We denote the contrastive loss for the i -th graph representation as:

$$\begin{aligned}
L_{g_i} &= \sum_{j=1}^N -\frac{e^{s(g_i, c_j)/\tau}}{\sum_{k=1}^N e^{s(g_i, c_k)/\tau}} \cdot \log \frac{e^{\delta(g_i, c_j)/\tau}}{\sum_{k=1}^N e^{\delta(g_i, c_k)/\tau}} \\
&= \sum_{j=1}^N -\text{softmax}(s(g_i, c_j)/\tau) \cdot \log(\text{softmax}(\delta(g_i, c_j)/\tau))
\end{aligned} \tag{5}$$

where $s(g_i, c_j) = ((\mathbf{h}_{g_i}^{\text{proj}})^T \cdot \mathbf{h}_{g_j}^{\text{proj}} + (\mathbf{h}_{c_i}^{\text{proj}})^T \cdot \mathbf{h}_{c_j}^{\text{proj}})/2$, $\delta(g_i, c_j) = (\mathbf{h}_{g_i}^{\text{proj}})^T \cdot \mathbf{h}_{c_j}^{\text{proj}}$, and τ is the temperature parameter. Similarly, the contrastive loss for the i -th chemical modality representation is:

$$L_{c_i} = \sum_{j=1}^N -\text{softmax}(s(g_j, c_i)/\tau) \cdot \log(\text{softmax}(\delta(g_j, c_i)/\tau)) \tag{6}$$

Such loss design aims to guarantee that irrespective of the input source, whether it originates from two modalities, the optimization procedure is oriented towards attaining consistent representations.

4.4 Datasets

4.4.1 Training Datasets

For molecular depiction image dataset, the molecules come from the Natural Products Magnetic Resonance Database (NPMRD) [58] and the images were produced by RDKit [59]. In total, there are about 270,000 samples in this dataset. For Smiles dataset, molecules and Smiles come from NPMRD as well. In total, there are about 270,000 samples in this dataset. For ^1H NMR dataset and ^{13}C NMR dataset, the molecules, ^1H NMR spectra and ^{13}C NMR spectra come from NPMRD as well. There are about 18,000 samples in ^1H NMR dataset, and 18,000 samples in ^{13}C NMR dataset. For GCMS dataset and LCMS dataset, molecules, LCMS spectra and GCMS spectra come from MassBank of North America (MoNA) [60]. There are about 10,000 samples in GCMS dataset, and 13,000 samples in LCMS dataset.

4.4.2 Zero-Shot Datasets

For the molecular candidate pool, 1M molecules were randomly chosen from PubChem, no intersection with training dataset. For the spectra, 1000 spectra were used from the validation dataset.

4.5 Training Details

For graph modality, each atom is embedded by its atomic number and chirality type, and each bond is embedded by its bond type and stereotype. We used GNNs with ReLU activation function and a sum pooling is applied on each graph as the final readout operation to extract the hidden graph representation. The best model settings are provided in Table 3. Besides GIN [44], we tried multiple convolution techniques and found that GCN [43] achieved similar results to GIN, whereas GAT [45] and GraphSage [46] degraded performance during validation. We noticed that the number of layers did not have a strong effect as long as it exceeded a value of 5, implying that a shallow graph encoder is expressive enough. For chemical modalities, we used pre-trained unimodal encoders according to Table 2, where each encoder keeps frozen in the training phase. Outputs from the graph encoder and the chemical unimodal encoder are projected into the same dimensional joint hidden space using a 2-layer MLP with a specific projection dimension as provided in Table 3. All models were optimized with AdamW [61] in Pytorch implementation with $\beta_1 = 0.9$, $\beta_2 = 0.999$, and weight decay of 0.001. The model is trained with a batch size of 128 for a total of 100 epochs. Each model is trained on one NVIDIA Tesla V100 GPU using float32 precision. The entire framework is training efficiently since only one shallow graph encoder and two MLPs from the projection module need to be updated through training.

Model	GNN type	# Layers	GNN hidden dim	Projection dim
G-Image	GIN	5	64	512
G-SMILES	GIN	5	64	512
G- ¹ HNMR	GIN	3	512	256
G- ¹³ CNMR	GIN	3	512	128
G-GCMS	GIN	5	128	128
G-LCMS	GIN	5	128	128

Table 3: Best Model settings.

5 Data availability

The pre-training data from NPMRD and MoNA, and the zero-shot PubChem dataset are publicly available online, well-organized, and can be directly downloaded. RDKit can assist in parsing the dataset into individual samples.

6 Code availability

We will publish our code in a later revision.

References

- [1] Liang, P. P., A. Zadeh, L.-P. Morency. Foundations and trends in multimodal machine learning: Principles, challenges, and open questions. 2023.
- [2] Ramesh, A., P. Dhariwal, A. Nichol, et al. Hierarchical text-conditional image generation with clip latents, 2022.
- [3] Alayrac, J.-B., J. Donahue, P. Luc, et al. Flamingo: a visual language model for few-shot learning. In S. Koyejo, S. Mohamed, A. Agarwal, D. Belgrave, K. Cho, A. Oh, eds., *Advances in Neural Information Processing Systems*, vol. 35, pages 23716–23736. Curran Associates, Inc., New York, 2022.
- [4] Sun, C., A. Myers, C. Vondrick, et al. Videobert: A joint model for video and language representation learning. In *Proceedings of the IEEE International Conference on Computer Vision*, pages 7464–7473. 2019.
- [5] Rombach, R., A. Blattmann, D. Lorenz, et al. High-resolution image synthesis with latent diffusion models. In *Proceedings of the IEEE/CVF Conference on Computer Vision and Pattern Recognition (CVPR)*, pages 10684–10695. 2022.
- [6] Brodeur, S., E. Perez, A. Anand, et al. Home: a household multimodal environment. In *NIPS 2017’s Visually-Grounded Interaction and Language Workshop*. 2017.
- [7] Savva, M., A. Kadian, O. Maksymets, et al. Habitat: A platform for embodied ai research. In *2019 IEEE/CVF International Conference on Computer Vision (ICCV)*, pages 9338–9346. 2019.
- [8] Zubatiuk, T., O. Isayev. Development of multimodal machine learning potentials: Toward a physics-aware artificial intelligence. *Accounts of Chemical Research*, 54(7):1575–1585, 2021.
- [9] Stahlschmidt, S. R., B. Ulfenborg, J. Synnergren. Multimodal deep learning for biomedical data fusion: a review. *Briefings in Bioinformatics*, 23(2):bbab569, 2022.
- [10] Kline, A., H. Wang, Y. Li, et al. Multimodal machine learning in precision health: A scoping review. *npj Digital Medicine*, 5(1):171, 2022.
- [11] Radford, A., J. W. Kim, C. Hallacy, et al. Learning transferable visual models from natural language supervision. 2021.
- [12] Kim, H., J. Lee, S. Ahn, et al. A merged molecular representation learning for molecular properties prediction with a web-based service. *Scientific Reports*, 11(1):11028, 2021.
- [13] Edwards, C., C. Zhai, H. Ji. Text2Mol: Cross-modal molecule retrieval with natural language queries. In *Proceedings of the 2021 Conference on Empirical Methods in Natural Language Processing*, pages 595–607. Association for Computational Linguistics, Online and Punta Cana, Dominican Republic, 2021.

[14] Pinheiro, G. A., J. L. F. Da Silva, M. G. Quiles. Smiclr: Contrastive learning on multiple molecular representations for semisupervised and unsupervised representation learning. *Journal of Chemical Information and Modeling*, 62(17):3948–3960, 2022.

[15] Wang, Y., J. Wang, Z. Cao, et al. Molecular contrastive learning of representations via graph neural networks. *Nature Machine Intelligence*, 4(3):279–287, 2022.

[16] Su, B., D. Du, Z. Yang, et al. A molecular multimodal foundation model associating molecule graphs with natural language. 2022.

[17] Ektefaie, Y., G. Dasoulas, A. Noori, et al. Multimodal learning with graphs. *Nature Machine Intelligence*, 5(4):340–350, 2023.

[18] Fang, Y., Q. Zhang, N. Zhang, et al. Knowledge graph-enhanced molecular contrastive learning with functional prompt. *Nature Machine Intelligence*, 5(5):542–553, 2023.

[19] Yang, Z., J. Song, M. Yang, et al. Cross-modal retrieval between ^{13}C nmr spectra and structures for compound identification using deep contrastive learning. *Analytical Chemistry*, 93(50):16947–16955, 2021.

[20] Clevert, D.-A., T. Le, R. Winter, et al. Img2mol—accurate smiles recognition from molecular graphical depictions. *Chemical science*, 12(42):14174–14181, 2021.

[21] Wang, Y., J. Wang, Z. Cao, et al. Molecular contrastive learning of representations via graph neural networks. *Nature Machine Intelligence*, 4(3):279–287, 2022.

[22] Weininger, D. Smiles, a chemical language and information system. 1. introduction to methodology and encoding rules. *Journal of chemical information and computer sciences*, 28(1):31–36, 1988.

[23] Zong, Y., O. M. Aodha, T. Hospedales. Self-supervised multimodal learning: A survey. 2023.

[24] Guo, H., K. Xue, H. Sun, et al. Contrastive learning-based embedder for the representation of tandem mass spectra. *Analytical Chemistry*, 95(20):7888–7896, 2023.

[25] Zeng, X., H. Xiang, L. Yu, et al. Accurate prediction of molecular properties and drug targets using a self-supervised image representation learning framework. *Nature Machine Intelligence*, 4(11):1004–1016, 2022.

[26] Li, C., J. Feng, S. Liu, et al. A novel molecular representation learning for molecular property prediction with a multiple smiles-based augmentation. *Computational Intelligence and Neuroscience*, 2022, 2022.

[27] Jiang, D., Z. Wu, C.-Y. Hsieh, et al. Could graph neural networks learn better molecular representation for drug discovery? a comparison study of descriptor-based and graph-based models. *Journal of cheminformatics*, 13(1):1–23, 2021.

[28] David, L., A. Thakkar, R. Mercado, et al. Molecular representations in ai-driven drug discovery: A review and practical guide. *Journal of Cheminformatics*, 12(1):56, 2020.

[29] Gilmer, J., S. S. Schoenholz, P. F. Riley, et al. Neural message passing for quantum chemistry. In *International conference on machine learning*, pages 1263–1272. PMLR, 2017.

[30] Wang, Y., S. Chen, G. Chen, et al. Motif-based graph representation learning with application to chemical molecules. In *Informatics*, vol. 10, page 8. MDPI, 2023.

[31] Guo, Z., B. Nan, Y. Tian, et al. Graph-based molecular representation learning. *arXiv preprint arXiv:2207.04869*, 2022.

[32] Jackson, J. E. *A user's guide to principal components*. John Wiley & Sons, 2005.

[33] Pearson, K. Notes on the history of correlation. *Biometrika*, 13(1):25–45, 1920.

[34] Yang, Z., J. Song, M. Yang, et al. Cross-modal retrieval between ^{13}C nmr spectra and structures for compound identification using deep contrastive learning. *Analytical Chemistry*, 93(50):16947–16955, 2021.

[35] Costanti, F., A. Kola, F. Scarselli, et al. A deep learning approach to analyze nmr spectra of sh-sy5y cells for alzheimer's disease diagnosis. *Mathematics*, 11(12):2664, 2023.

[36] Wu, Z., S. Pan, F. Chen, et al. A comprehensive survey on graph neural networks. *IEEE transactions on neural networks and learning systems*, 32(1):4–24, 2020.

[37] Zhou, J., G. Cui, S. Hu, et al. Graph neural networks: A review of methods and applications. *AI open*, 1:57–81, 2020.

[38] LeCun, Y., Y. Bengio, G. Hinton. Deep learning. *nature*, 521(7553):436–444, 2015.

[39] Baskin, I. I., V. A. Palyulin, N. S. Zefirov. A neural device for searching direct correlations between structures and properties of chemical compounds. *Journal of chemical information and computer sciences*, 37(4):715–721, 1997.

[40] Sperduti, A., A. Starita. Supervised neural networks for the classification of structures. *IEEE Transactions on Neural Networks*, 8(3):714–735, 1997.

[41] Gori, M., G. Monfardini, F. Scarselli. A new model for learning in graph domains. In *Proceedings. 2005 IEEE International Joint Conference on Neural Networks, 2005.*, vol. 2, pages 729–734. IEEE, 2005.

[42] Kearnes, S., K. McCloskey, M. Berndl, et al. Molecular graph convolutions: moving beyond fingerprints. *Journal of computer-aided molecular design*, 30:595–608, 2016.

[43] Kipf, T. N., M. Welling. Semi-supervised classification with graph convolutional networks. In *International Conference on Learning Representations*. 2017.

[44] Xu, K., W. Hu, J. Leskovec, et al. How powerful are graph neural networks? In *International Conference on Learning Representations*. 2019.

[45] Velickovic, P., G. Cucurull, A. Casanova, et al. Graph attention networks. *stat*, 1050(20):10–48550, 2017.

[46] Hamilton, W., Z. Ying, J. Leskovec. Inductive representation learning on large graphs. *Advances in neural information processing systems*, 30, 2017.

[47] Gu, J., Z. Wang, J. Kuen, et al. Recent advances in convolutional neural networks. *Pattern recognition*, 77:354–377, 2018.

[48] Cangea, C., P. Veličković, N. Jovanović, et al. Towards sparse hierarchical graph classifiers. *arXiv preprint arXiv:1811.01287*, 2018.

[49] Ying, Z., J. You, C. Morris, et al. Hierarchical graph representation learning with differentiable pooling. *Advances in neural information processing systems*, 31, 2018.

[50] Vinyals, O., S. Bengio, M. Kudlur. Order matters: Sequence to sequence for sets. *arXiv preprint arXiv:1511.06391*, 2015.

[51] Zhang, M., Z. Cui, M. Neumann, et al. An end-to-end deep learning architecture for graph classification. In *Proceedings of the AAAI conference on artificial intelligence*, vol. 32. 2018.

[52] Corso, G., L. Cavalleri, D. Beaini, et al. Principal neighbourhood aggregation for graph nets. *Advances in Neural Information Processing Systems*, 33:13260–13271, 2020.

[53] Buterez, D., J. P. Janet, S. J. Kiddle, et al. Graph neural networks with adaptive readouts. *Advances in Neural Information Processing Systems*, 35:19746–19758, 2022.

[54] Tailor, S. A., F. Opolka, P. Lio, et al. Do we need anisotropic graph neural networks? In *International Conference on Learning Representations*. 2022.

[55] Zolfaghari, M., Y. Zhu, P. Gehler, et al. Crossclr: Cross-modal contrastive learning for multi-modal video representations. In *Proceedings of the IEEE/CVF International Conference on Computer Vision*, pages 1450–1459. 2021.

[56] Morgado, P., N. Vasconcelos, I. Misra. Audio-visual instance discrimination with cross-modal agreement. In *Proceedings of the IEEE/CVF Conference on Computer Vision and Pattern Recognition*, pages 12475–12486. 2021.

[57] Shariatnia, M. M. Simple CLIP, 2021.

[58] Wishart, D. S., Z. Sayeeda, Z. Budinski, et al. Np-mrd: the natural products magnetic resonance database. *Nucleic Acids Research*, 50(D1):D665–D677, 2022.

[59] RDKit: Open-source cheminformatics. <http://www.rdkit.org>.

[60] Massbank of north america (mona).

[61] Loshchilov, I., F. Hutter. Decoupled weight decay regularization. *arXiv preprint arXiv:1711.05101*, 2017.